

This site uses cookies. By continuing to use this site you agree to our use of cookies. To find out more, see our [Privacy and Cookies policy](#).



NOTICE: Ensuring subscriber access to content on IOPscience throughout the coronavirus outbreak - see our [remote access guidelines](#).

Table of contents

Volume 21

Number 6, September 2013

[◀ Previous issue](#) [Next issue ▶](#)

[Buy this issue in print](#)

[Open all abstracts](#)

Review Article

Molecular modeling of protein materials: case study of elastin 063001

Anna Tarakanova and Markus J Buehler

[+ Open abstract](#) [View article](#) [PDF](#)

Papers

Mechanisms of anisotropic friction in nanotwinned Cu revealed by atomistic simulations 065001

J J Zhang, A Hartmaier, Y J Wei, Y D Yan and T Sun

[+ Open abstract](#) [View article](#) [PDF](#)

Molecular dynamics simulation of the initial stages of He bubbles formation in silicon 065002

L Pizzagalli, M L David and M Bertolus

[+ Open abstract](#) [View article](#) [PDF](#)

Gupta potential for rare earth elements of the fcc phase: lanthanum and cerium 065003

Jie Fu and Jijun Zhao

[+ Open abstract](#) [View article](#) [PDF](#)

Determination of depths of traps for interstitials from thermodynamic data: a new view on carbon trapping and diffusion 065012

J Svoboda, Y V Shan, E Kozeschnik and F D Fischer

[+ Open abstract](#) [View article](#) [PDF](#)

Use of spherical harmonics for dislocation dynamics in anisotropic elastic media 065013

S Aubry and A Arsenlis

[+ Open abstract](#) [View article](#) [PDF](#)

Thermal properties of UO_2 with a non-local exchange-correlation pressure correction: a systematic first principles DFT + U study 065014

Gurpreet Kaur, Puspamitra Panigrahi and M C Valsakumar

[+ Open abstract](#) [View article](#) [PDF](#)

Semiconductor to metal transition in bilayer transition metals dichalcogenides MX_2 ($M = \text{Mo}, \text{W}; X = \text{S}, \text{Se}, \text{Te}$) 065015

Ashok Kumar and P K Ahluwalia

[+ Open abstract](#) [View article](#) [PDF](#)

Effects of temperature and strain rate on the deformation of amorphous polyethylene: a comparison between molecular dynamics simulations and experimental results 065016

I H Sahputra and A T Echtermeyer

[+ Open abstract](#) [View article](#) [PDF](#)

Influence of temperature and free edges on the mechanical properties of graphene 065017

M A N Dewapriya, A Srikantha Phani and R K N D Rajapakse

[+ Open abstract](#) [View article](#) [PDF](#)

Study of architectural responses of 3D periodic cellular materials 065018

Yigil Cho, Tae-Hong Ahn, Hoon-Hwe Cho, Joong-Ho Shin, Jun Hyuk Moon, Shu Yang, In-Suk Choi, Heung Nam Han and Ju Li

[+ Open abstract](#) [View article](#) [PDF](#)

Atomistic study of stress-induced switching of 90° ferroelectric domain walls in PbTiO_3 : size, temperature and structural effect 065019

A Kubo, J-M Albina and Y Umeno

[+ Open abstract](#) [View article](#) [PDF](#)



Ukraine: Click here to read IOP Publishing's statement



Modelling and Simulation in Materials Science and Engineering

Journals > Editorial board

Follow:



[Homepage](#)

[Author guidelines](#)

[About Modelling and Simulation in Materials Science and Engineering](#)

[Editorial board](#)

[Track my article](#)

Editorial board

The Editorial Board works with the in-house editorial team to ensure the journal meets its aim of high quality peer review, rapid publication and inclusive subject coverage. Leaders in their fields, they provide final arbitration for scientific disputes and support the rapid peer review of author manuscripts.

In 2020 we welcomed our new Editor-in-Chief, Javier Llorca. We took this opportunity to interview Javier about his vision for the journal, read the interview [here](#).

Editor-in-Chief

Javier Llorca Polytechnic University of Madrid & IMDEA Materials Institute, Spain

Executive Editorial Board

Youping Chen University of Florida, USA

Anthony Rollett Carnegie Mellon University, USA

David Srolovitz University of Pennsylvania, USA

Yujie Wei Chinese Academy of Sciences, China

Yong-Wei Zhang A*STAR Institute of High Performance Computing, Singapore

Editorial Board

Michael I Baskes Mississippi State University, USA

Richard Becker US Army Medical Research and Material Command, USA

Michel Bellet Ecole des Mines de Paris, France

Yves Bréchet Institut National Polytechnique de Grenoble, France

Vasily Bulatov Lawrence Livermore National Laboratory, USA

Wei Cai Stanford University, USA

Abhijit Chatterjee Indian Institute of Technology Bombay, India

Vikram Deshpande University of Cambridge, UK

Somnath Ghosh John Hopkins University, USA

Erik van der Giessen University of Groningen, The Netherlands

Peter Gumbsch Fraunhofer-Institut für Werkstoffmechanik, Germany

Håkan Hallberg Lund University, Sweden

Seungwu Han Seoul National University, South Korea

Abigail Hunter Los Alamos National Laboratory, USA

Masanori Kohyama National Institute of Advanced Industrial Science and Technology, Japan

Yuri Mishin George Mason University, USA

Dan Mordehai Technion University, Israel

Tim Mueller John Hopkins University, USA

Alfonso Ngan Hong Kong University, Hong Kong

Lucia Nicola Delft University of Technology, The Netherlands

Marta Oliveira University of Coimbra, Portugal

Danny Perez Los Alamos National Laboratory, USA

Dierk Raabe Max-Planck-Institut für Eisenforschung, Düsseldorf, Germany

Joerg Rottler University of British Columbia, Canada

Robert Rudd Lawrence Livermore National Laboratory, USA

Katrin Schulz Karlsruhe Institute of Technology, Germany

Ingo Steinbach Ruhr-Universität-Bochum, Germany

Alejandro Strachan Purdue University, USA

Alexander Urban Columbia University, USA

Muhammad Usman University of Melbourne, Australia

Francois Willaime CEA-Saclay Reserach Centre, France

Dongsheng Xu Chinese Academy of Sciences, China

Yang Xiang Hong Kong University of Science and Technology, Hong Kong

Ruifeng Zhang Beihang University, China

Editorial board

[Back to top](#)

[Back to top](#)

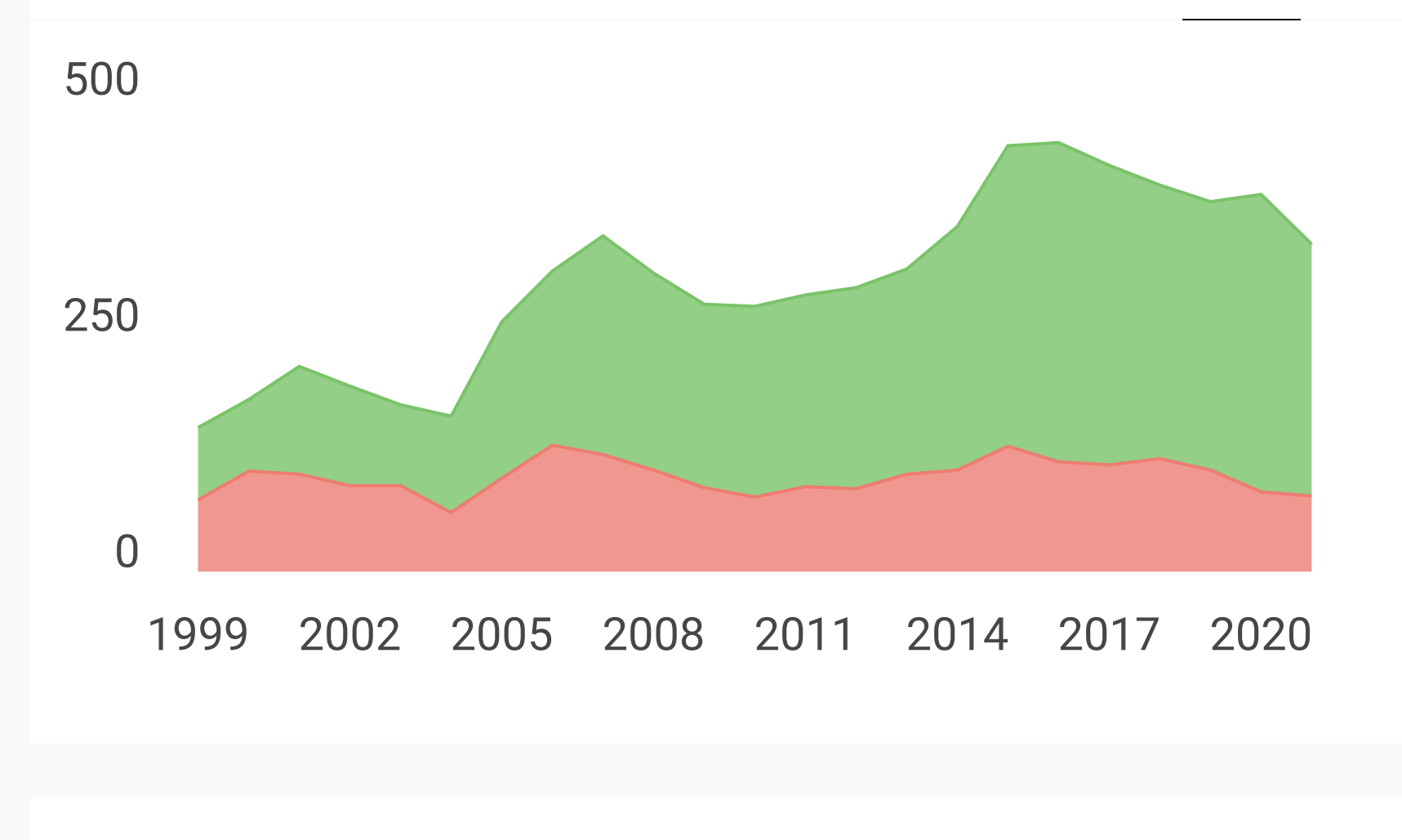
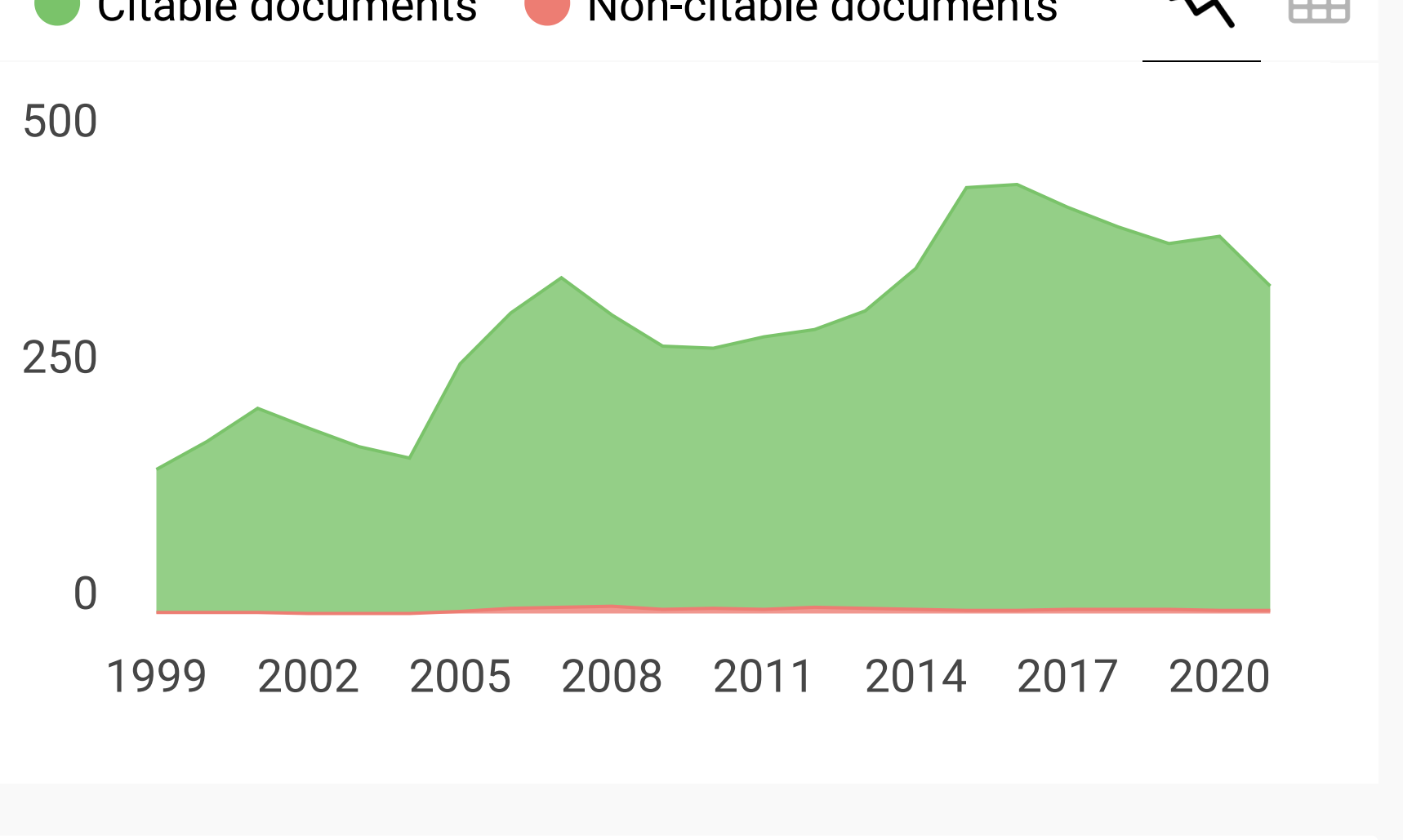
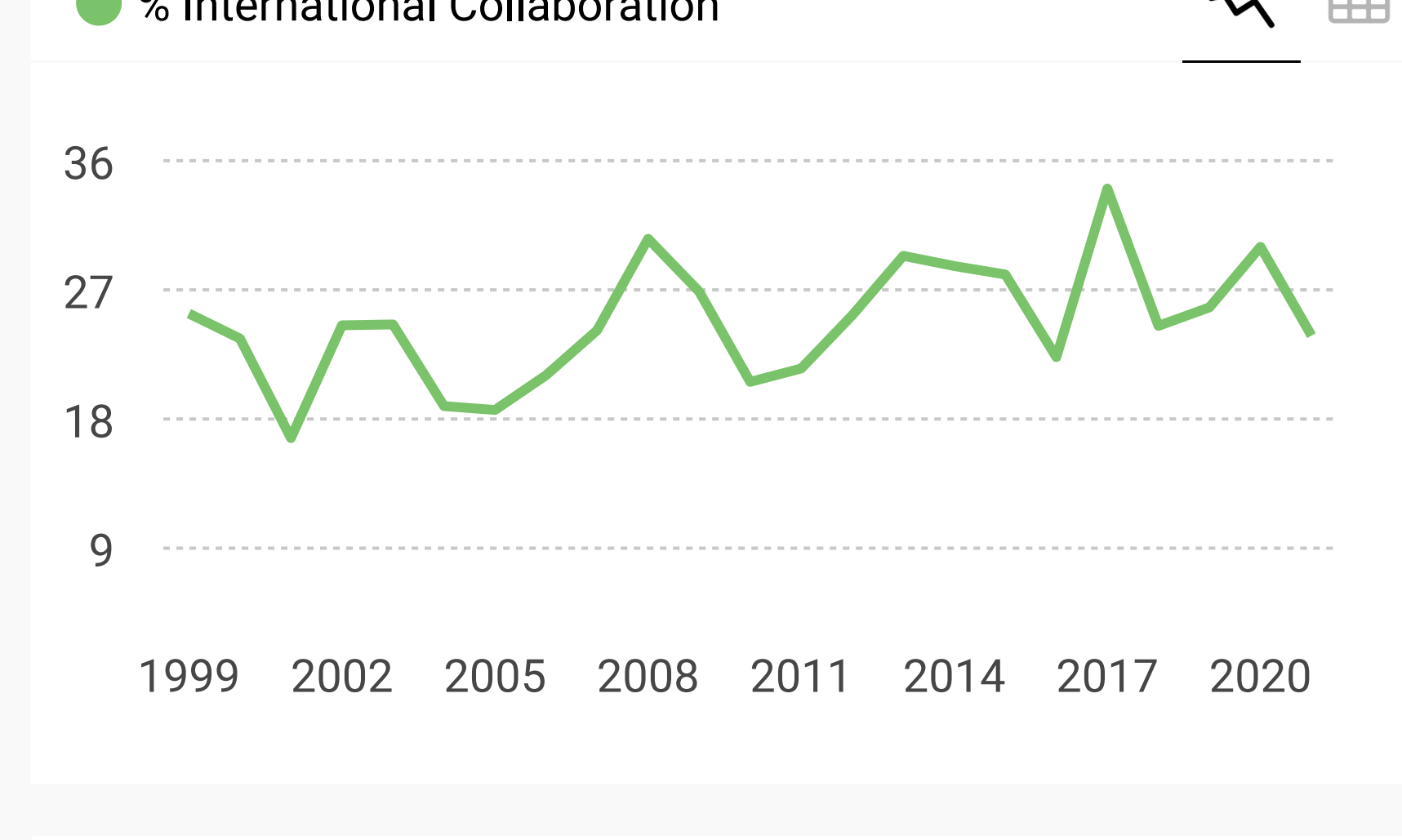
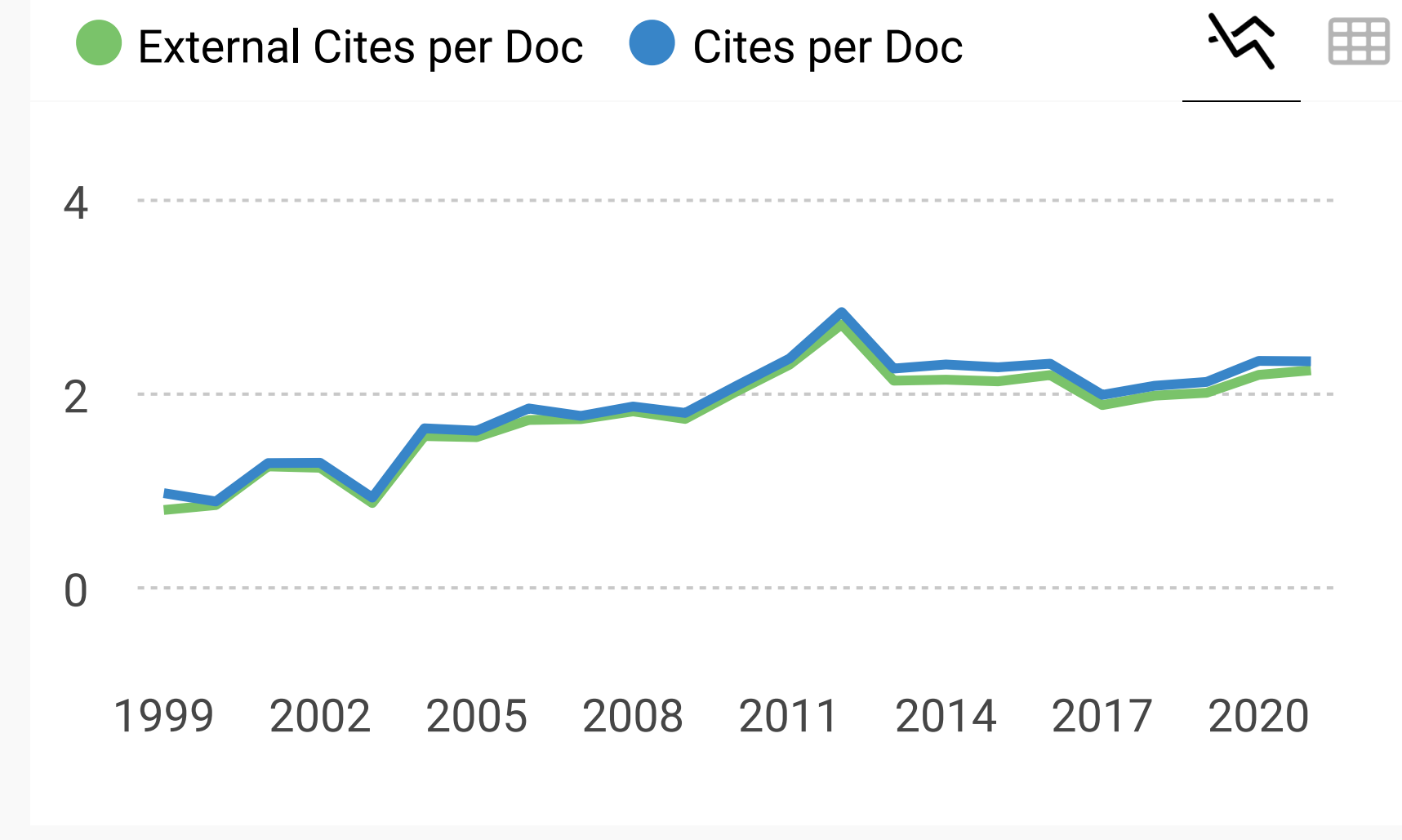
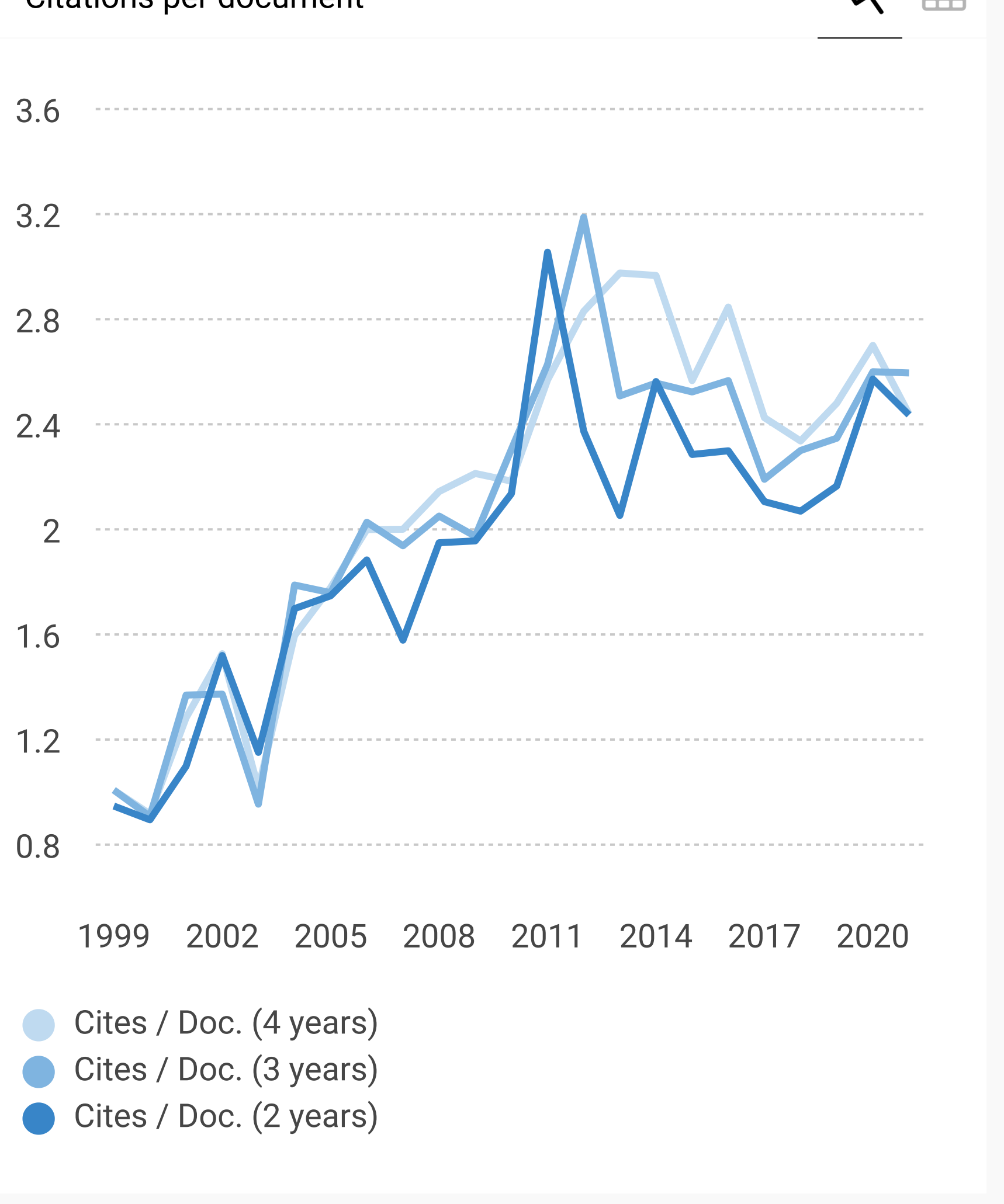
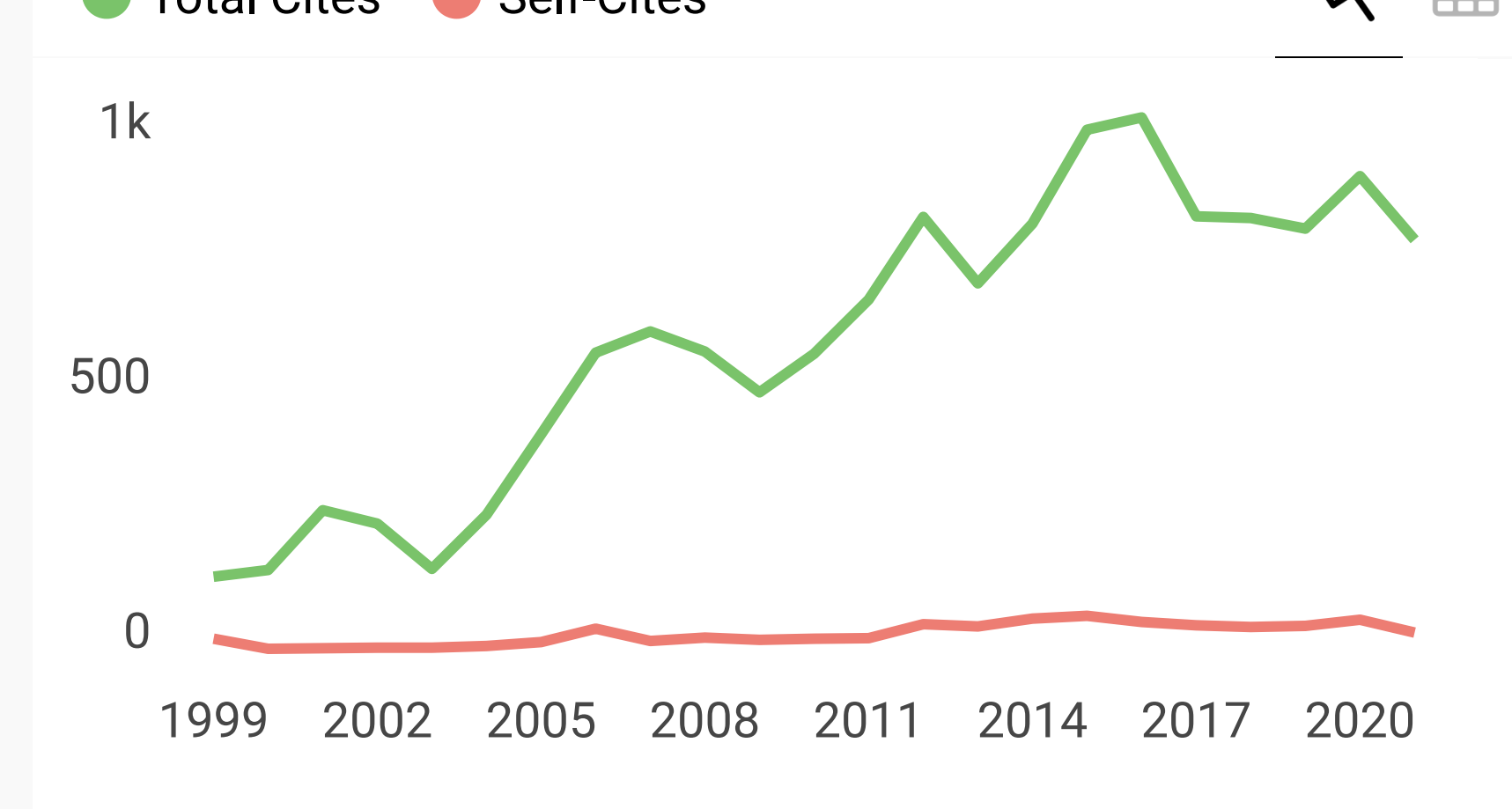
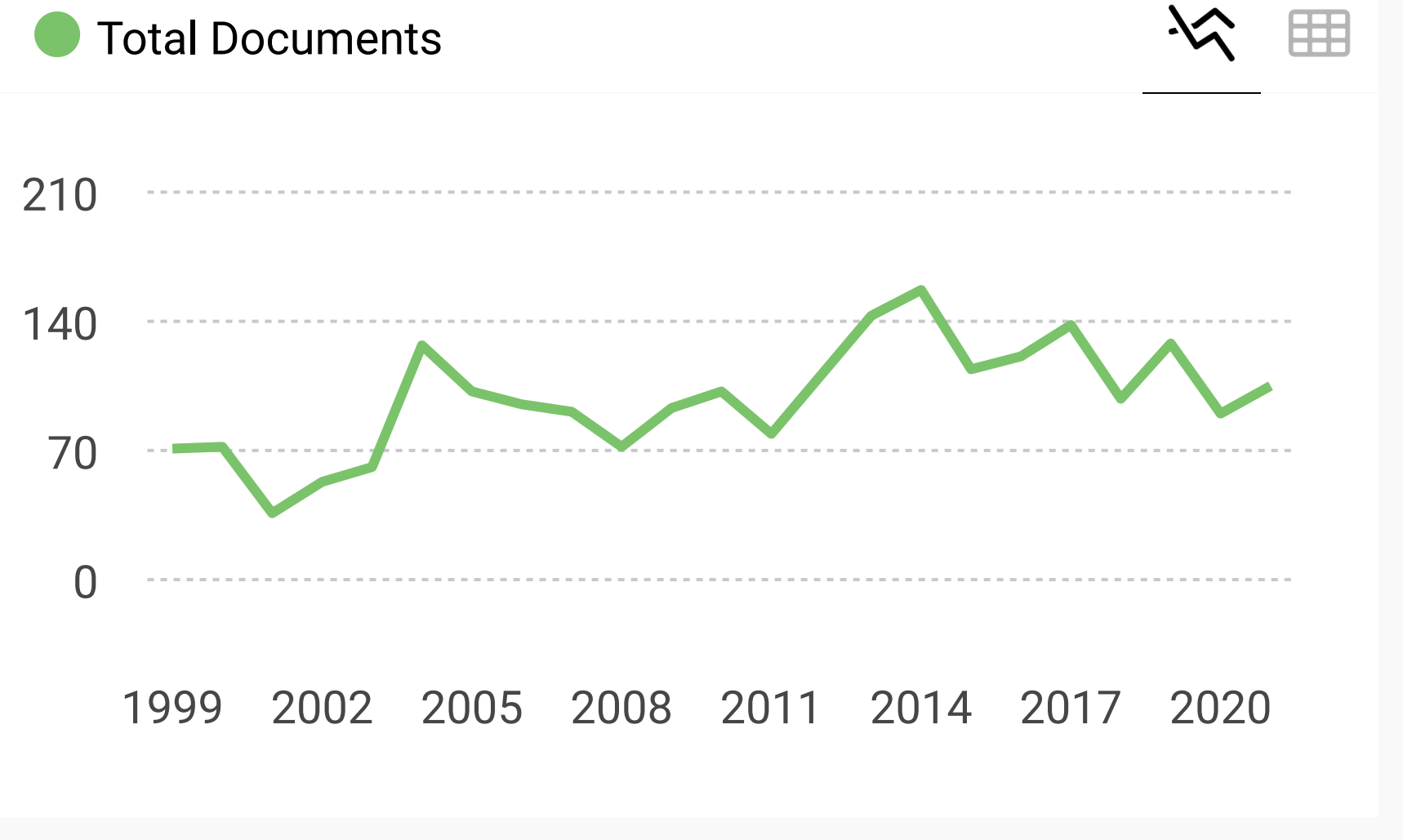
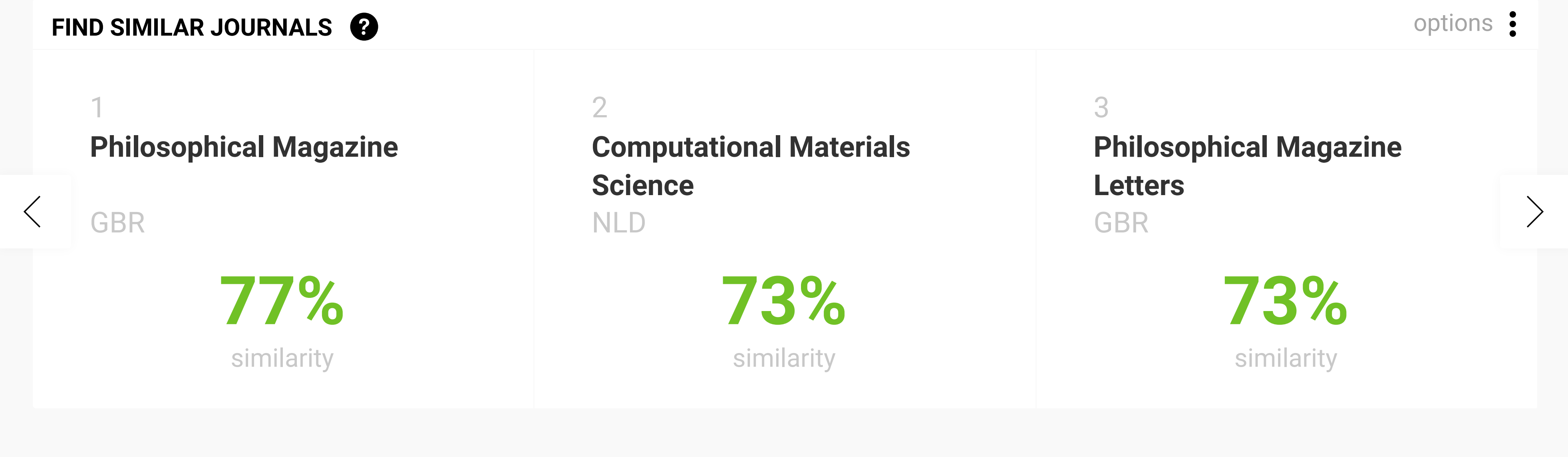
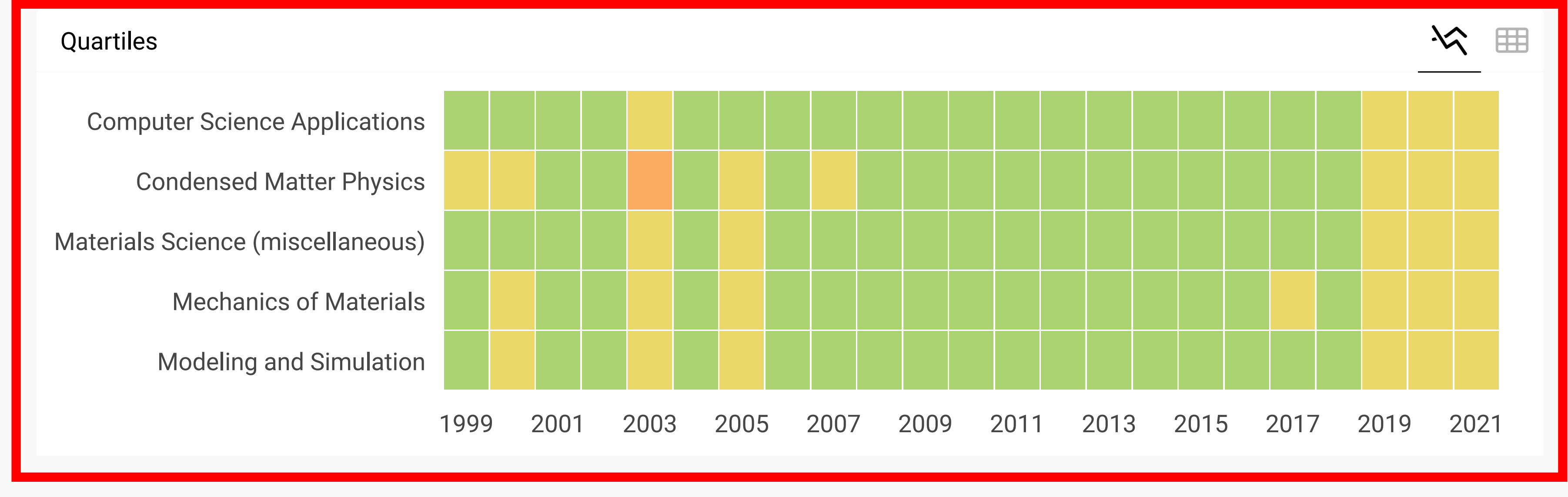
Modelling and Simulation in Materials Science and Engineering

<p>COUNTRY</p> <p>United Kingdom</p> <p> Universities and research institutions in United Kingdom</p>	<p>SUBJECT AREA AND CATEGORY</p> <ul style="list-style-type: none"> Computer Science <ul style="list-style-type: none"> Computer Science Applications Engineering <ul style="list-style-type: none"> Mechanics of Materials Materials Science <ul style="list-style-type: none"> Materials Science (miscellaneous) Mathematics <ul style="list-style-type: none"> Modeling and Simulation Physics and Astronomy <ul style="list-style-type: none"> Condensed Matter Physics 	<p>PUBLISHER</p> <p>IOP Publishing Ltd.</p>
<p>H-INDEX</p> <p>84</p>	<p>PUBLICATION TYPE</p> <p>Journals</p>	<p>ISSN</p> <p>09650393, 1361651X</p>
<p>COVERAGE</p> <p>1992-2021</p>	<p>INFORMATION</p> <p>Homepage</p> <p>How to publish in this journal</p> <p>paschul@sandia.gov</p>	

SCOPE

Serving the multidisciplinary materials community, the journal aims to publish new research work that advances the understanding and prediction of material behaviour at scales from atomistic to macroscopic through modelling and simulation. Subject coverage: Modelling and/or simulation across materials science that emphasizes fundamental materials issues advancing the understanding and prediction of material behaviour. Interdisciplinary research that tackles challenging and complex materials problems where the governing phenomena may span different scales of materials behaviour, with an emphasis on the development of quantitative approaches to explain and predict experimental observations. Material processing that advances the fundamental materials science and engineering underpinning the connection between processing and properties. Covering all classes of materials, and mechanical, microstructural, electronic, chemical, biological, and optical properties.

Join the conversation about this journal



Modelling and Simulation in Materials Science and... [Show this widget in your own website](#)

Q2 Computer Science Applications
best quartile

SJR 2021
0.62

powered by scimagojr.com

Just copy the code below and paste within your html code:

ScImago Graphica

Explore, visually communicate and make sense of data with our [new data visualization tool](#).

Metrics based on Scopus® data as of April 2022

Leave a comment

Name

Email (will not be published)

The users of Scimago Journal & Country Rank have the possibility to dialogue through a specific journal. The purpose is to have a forum in which general doubts about the processes of publication in the journal, experiences and other issues derived from the publication of papers are resolved. For topics on particular articles, maintain the dialogue through the usual channels with your editor.

Effects of temperature and strain rate on the deformation of amorphous polyethylene: a comparison between molecular dynamics simulations and experimental results

This article has been downloaded from IOPscience. Please scroll down to see the full text article.

2013 Modelling Simul. Mater. Sci. Eng. 21 065016

(<http://iopscience.iop.org/0965-0393/21/6/065016>)

View [the table of contents for this issue](#), or go to the [journal homepage](#) for more

Download details:

IP Address: 131.211.208.19

The article was downloaded on 03/09/2013 at 07:25

Please note that [terms and conditions apply](#).

Effects of temperature and strain rate on the deformation of amorphous polyethylene: a comparison between molecular dynamics simulations and experimental results

I H Sahputra and A T Echtermeyer

Engineering Design and Materials Department, Norwegian University of Science and Technology-NTNU, Trondheim, Norway

E-mail: iwan.h.sahputra@ntnu.no

Received 3 December 2012, in final form 25 June 2013

Published 8 August 2013

Online at stacks.iop.org/MSMSE/21/065016

Abstract

Molecular dynamics simulations are used to investigate the effects of temperature and strain rate on the deformation of amorphous polyethylene. The simulations predict the effects of temperature and strain rate on the stress–strain responses, Young’s modulus and Poisson’s ratio similar to those observed in laboratory experiments performed by other researchers. The time–temperature superposition principle is applied to the Young’s modulus and Poisson’s ratio to form a master curve to address the discrepancies in strain rates between the simulations and the experiments. Differences in the numbers of monomers and chains, the degree of crystallinity and molecular orientation lead to discrepancies in the Young’s modulus and Poisson’s ratio between simulations and experiments.

1. Introduction

Molecular dynamics (MD) can predict material properties based on first principles, mainly using the atomistic forces between molecules. This approach could help in the design of new materials by modelling the behaviour of materials with altered molecular structures. The user could predict material performance under different loads and environments without performing traditional physical experiments in the laboratory. MD modelling of polymers has not yet reached this level. Current computational power is not sufficient to model the many macromolecules in polymeric materials and describe all the interactions within a reasonable time frame. This particularly applies to the modelling of long-term properties such as creep and fatigue.

This paper investigates as to what extent temperature and strain rate effects can be described by MD. In particular, we investigate the possibility of using the time–temperature superposition

principle. High-density polyethylene (HDPE) is used for this investigation. HDPE has a simple molecular structure, even though it has amorphous and crystalline phases, and this polymer is employed in a wide range of demanding industrial applications, for example, in gas distribution pipes [1].

Several MD studies have been performed to investigate the behaviour of polyethylene (PE). Brown and Clark [2] modelled a single linear polymer containing 1000 monomers of PE in tension, performing simulations at different loading rates and temperatures. By qualitative comparison, they observed similar stress–strain responses between the simulations and laboratory measurements carried out at much lower strain rates.

Yang *et al* [3] presented simulations of 1500 atoms of PE arranged in 5 chains of equal length. Their simulation produced a similar Young's modulus value as reported by Brown and Clark [2]. However, the simulated yield stress/strain and the ultimate strength predicted by these simulations were much higher than those obtained from laboratory experiments at a strain rate approximately six orders of magnitude smaller.

Capaldi *et al* [4] used non-equilibrium MD simulations to simulate four chains with 1000 beads representing PE monomers at a variety of temperatures and strain rates. They found that their simulations were able to qualitatively reproduce the experimentally observed stress–strain behaviour of polymer glasses during compressive deformation. They also demonstrated that the simulated modulus is consistent with the experimentally determined modulus, but the yield stress was much higher.

Rottler and Robbins [5] studied the effect of temperature and strain rate on shear yielding of amorphous glassy solids. A bead–spring model was used for non-particular polymers and the other model was a binary mixture composed of two particles. Both models were subjected to tensile or compressive strains with strain rates much higher than typical experimental tests. They found that the maximum shear yield stress drops linearly with increasing temperature and the dependence on strain rate can be described by either a logarithm or a power law added to a constant.

Mahajan and Basu [6] investigated the effects of sample preparation, quench rate, sample size and strain rate on the ensemble and stress–strain response. They used a force field and mass of atoms that closely resembles that of PE and performed uniaxial compression simulations. They showed the sample preparation and simulation procedures, which were able to produce realistic stress–strain curves with strain rates much higher compared with the experimental tests.

Lyulin *et al* [7] used united-atom models to simulate uniaxial deformation of low-molecular weight isopropylbenzene (iPB), brittle atactic polystyrene (PS) and tough bisphenol A polycarbonate (PC). After the deformation simulation at room temperature, they found the Young's modulus and yield stress values close to the typical value obtained from the experimental results at the same temperature; however, there was huge discrepancy in the strain rates.

These previous results indicate that MD is a useful tool to qualitatively investigate the relationship between micro-scale phenomena and macro-scale mechanical properties and, to some extent, to quantitatively determine these terms. However, there is a huge discrepancy between the simulated and laboratory strain rates. Because of the computational cost and time required, MD simulations typically use strain rates about 6 to 10 orders of magnitude larger than the highest strain rates commonly used in laboratory experiments.

This study will investigate the effects of temperature and strain rate on the deformation mechanisms of amorphous PE using MD simulations. This investigation will further explore the ability of MD simulations to serve as a tool, not only to produce results that are qualitatively similar to experimental results, but also to provide quantitative results. This is done by

Table 1. Functional forms and parameters for molecular potential energy.

Interaction	Functional form	Parameters
Bond stretch	$V_b = k_b(r_b - r_o)^2$	$k_b = 350 \text{ kcal mol}^{-1}$ $r_b = \text{bond length}$ $r_o = \text{equilibrium bond length} = 1.53 \text{ \AA}$
Bond angle bend	$V_a = k_a(\theta_a - \theta_b)^2$	$k_a = 60 \text{ kcal mol}^{-1}$ $\theta_a = \text{bond angle}$ $\theta_b = \text{equilibrium bond angle} = 109.5^\circ$
Dihedral angle torsion	$V_d = \sum_{n=1}^4 k_n \cos^{n-1} \phi_d$	$K_1 = 1.73 \text{ kcal mol}^{-1}$, $K_2 = -4.49 \text{ kcal mol}^{-1}$ $K_3 = 0.776 \text{ kcal mol}^{-1}$, $K_4 = 6.99 \text{ kcal mol}^{-1}$ $\phi_d = \text{dihedral angle}$
van der Waals	$V_{ij} = 4\varepsilon_{ij} \left[\left(\frac{\sigma_{ij}}{r_{ij}} \right)^{12} - \left(\frac{\sigma_{ij}}{r_{ij}} \right)^6 \right]$, $r < r_c$	$\varepsilon_{ij} = 0.112 \text{ kcal mol}^{-1}$, $\sigma_{ij} = 4.01 \text{ \AA}$ $r_c = 10 \text{ \AA}$

comparing the dependence of the simulated Young's modulus and Poisson's ratio on the temperature and strain rate with the dependences observed in laboratory experiments performed by other researchers. Discrepancies in strain rates between simulations and laboratory experiments will be discussed.

2. Model and simulation procedure

Pure PE consists of alkanes, and its chemical formula is $(\text{CH}_2)_n$, where n is the degree of polymerization or the number of ethylene monomers. The typical degree of polymerization of PE is between 100 and 250 000 or more. The molecular weight of PE is 14.02 per monomer. A PE sample consists of a large number of chains with a range of different lengths. HDPE has the chemical structure closest to pure PE because it consists primarily of unbranched PE molecules compared with other types of PE such as low-density polyethylene (LDPE).

The united-atom approach was used to model the amorphous PE system. This approach simplifies each CH_2 monomer as a single monomer particle and has been used by several researchers [2–4]. The DREIDING force field [8] was used to simulate the interaction between monomers. In DREIDING, the potential energy of a molecule consists of the combined energies of bonded interactions (bond stretching, bond angle bending and dihedral angle torsion) and non-bonded interactions (van der Waals interactions, represented by the Lennard-Jones potential). The functional forms and parameters [9, 10] of the DREIDING force field are presented in table 1.

The initial amorphous PE sample was generated using Monte Carlo self-avoiding random walks similar to previously developed methods [10]. The basic idea of this method is each monomer is placed on each site of the face-centred cubic (fcc) lattice with a lattice constant of 1.53 Å. The initial position is randomly selected and the next atom is placed according to the probability for each possible bond angle direction and the density of unoccupied neighbour sites. The sample contains ten chains, each consisting of 1000 monomers. An MD program designed for parallel computers, LAMMPS [11], was used to equilibrate the initial sample structure and simulate the deformation process. All the simulations were performed on the 'Njord' IBM p575+ super computer system at NTNU. This simulation represents the most complex simulation that can be performed on our supercomputer within a reasonable time frame, but it is a very small sample compared with real PE.

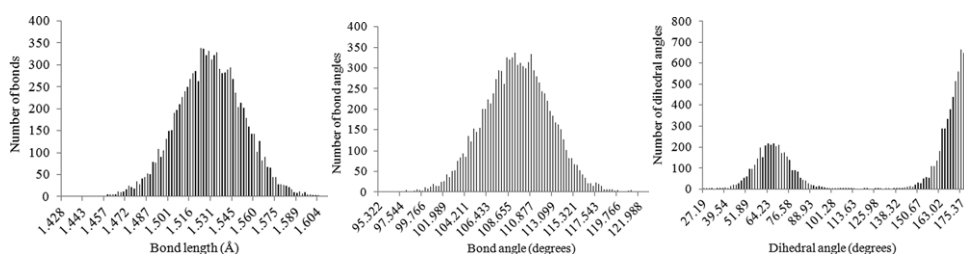


Figure 1. Distribution of the bond length, bond angle and dihedral angle after the final equilibration stage at a temperature of 200 K.

The simulation method used here followed that in [10]. Initial velocities were assigned to the atoms by randomly selecting from a uniform distribution at a temperature of 500 K. Before the deformation process, the system was equilibrated using a Langevin thermostat as described in [12] for 10 picoseconds (ps) at 500 K. The Langevin thermostats follow the Langevin equation of motion, where a frictional force proportional to the velocity is added to the conservative force, adjusting the kinetic energy of the particle so that the temperature matches the set temperature [13]. This thermostat was used within NVE ensembles to perform Brownian dynamics simulation of the melted polymer. The system was then equilibrated at constant particle number, pressure and temperature (NPT ensembles) for 25 ps at 500 K and then cooled to the desired temperature (100, 200, 250 and 350 K) for 25 ps. The final equilibration stage was carried out for NPT ensembles at the desired temperatures for 25 ps.

The NPT ensembles were performed using a Nose–Hoover thermostat and a barostat coupled to the atom velocities and simulation box dimensions. The time integration of the motion equations was performed using the time-reversible measure-preserving Verlet and rRESPA integrators. Periodic boundary conditions were applied to all directions of the simulation box.

During the sample preparation processes, pressure and stress were monitored to characterize whether equilibration has been satisfied. In the final equilibration stage, all the potential energies (bond, angle, dihedral and van der Waals) and polymer chain geometries were also monitored to check whether the final equilibrium was reached and the sample was ready to be deformed. Figure 1 shows an example of the polymer chain geometry after the final equilibration stage at a temperature of 200 K. The mean value of bond length is 1.529 Å with a standard deviation of 0.023 Å, while the mean value of bond angle is 109.29° with a standard deviation of 3.393°. These mean values are slightly lower than the equilibrium values of the potential parameters for bond length and angle, which are 1.53 Å and 109.5°, respectively. The dihedral angles are distributed around trans and gauche states, centred around 66° and 180°. The distributions are similar to those in other MD simulations of PE [6, 10].

A polymer's size can be characterized by the end-to-end distance, r , or the radius of gyration. For the freely jointed chain model, the end-to-end distance, r , is proportional to the bond length, l , and to the square root of the number of bonds, n . The characteristic ratio is defined as

$$C = \frac{\langle r^2 \rangle}{nl^2}. \quad (1)$$

In the freely jointed PE chain, $C = 1$, in the freely rotating chain, $C = 2$, and in the hindered rotation chain, $C = 3.4$ [14]. For real PE, the characteristic ratios are estimated from direct intrinsic viscosity measurements to be 7.10, 6.99 and 6.80 at temperatures of 127.5 °C, 142.2 °C

and 163.9°C, respectively [15]. In more recent light scattering measurements on linear PE in diphenyl at 400 K (= 127°C), characteristic ratios from 8.7 to 10.5 were found [16]. The sample of this study, after being equilibrated at a temperature of 500 K (= 227°C) has a characteristic ratio, C , of 3.4. This indicates that the simulation sample is composed of more tightly coiled chains compared with the real PE.

The accuracy of the stress–strain response of glassy polymers with MD simulations depends on the characteristic ratio, C [6]. However, the accuracy of C is especially important for the stress–strain response after the yield stress and for the slope of the rehardening part. The initial low strain is not influenced significantly by the value of C . As the focus of this study is on the Young's modulus and Poisson's ratio calculated at a low strain (0.02% or 2%), only the initial deformation responses of the simulations are used to calculate the elastic properties. For this reason, the model is considered adequate for studying elastic properties at low strains. However, this model is not an adequate model to predict properties beyond the elastic limit, such as the yield stress, softening and hardening, which is typically also beyond the practical application of polymers.

Deformation was simulated by changing the simulation box in one longitudinal direction during a dynamic run. The other two transverse directions of the box had zero applied pressure, allowing the box to contract sideways. The change in longitudinal dimension occurred at a constant engineering strain rate. The tensile strain is unitless and is defined as the length change divided by the original box length.

For each combination of temperature and strain rate, three simulations were performed to calculate the Young's modulus and Poisson's ratio. In each of the three simulations, the system was either elongated in the X , Y or Z direction and the obtained Young's modulus and Poisson's ratio were averaged. This was done because the initial structure and velocities were randomly generated, and after the equilibrium processes, the system could have different morphological configurations. This is similar to the practice of using several samples in laboratory experiments to ensure that the results are statistically representative of the material properties, which could vary.

3. Results and discussion

3.1. Effects of temperature and strain rate on the stress–strain curve and volume strain

Figure 2 presents typical stress–strain curves obtained from the simulations performed in this study. The simulations were conducted using a strain rate of 10^9 s^{-1} at a temperature of 200 K. The stress–strain curves were obtained from three simulations in which the sample was elongated in the X , Y or Z direction in each simulation. The heterogeneity and small size of the sample produced noisy stress–strain curves and therefore polynomial smoothing was used to reduce the fluctuation of the stress. This was done by applying the polynomial equations to the original stress–strain data and by calculating the least-squares fit through the data points.

The three curves are close to each other at a low strain. At a higher strain, above approximately 0.2% or 20%, the curves demonstrate that the stress–strain responses of the sample differ depending on the direction of elongation. This is due to the anisotropy of the structure of the polymer chain in the small sample modelled here. As the focus of this study is on the Young's modulus and Poisson's ratio calculated at a low strain (0.02 or 2%), similar initial deformation responses of the simulations in three different directions could be used to calculate the elastic properties. But this small model is not an adequate model to simulate large strain beyond the elastic limit, which is typically also beyond the practical application

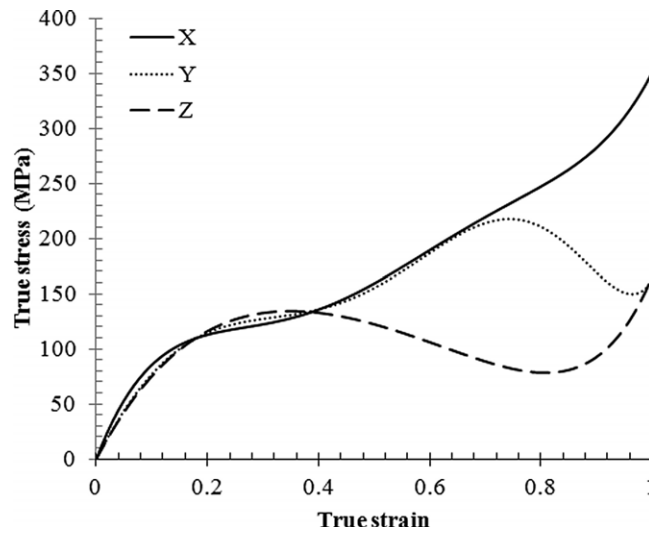


Figure 2. Stress–strain curves of three simulations elongated in the X, Y or Z direction at a strain rate of 10^9 s^{-1} at 200 K. The main focus in this study is on the initial strain range up to about 0.02% or 2%.

of polymers. For the following discussion in this section, only stress–strain curves from the deformation along the X-direction will be shown.

The curve for X-direction elongation in figure 2 has the same typical shape as those obtained from laboratory experiments on PE, for instance, the experiments using strain rates between 10^{-4} and 10^{-2} s^{-1} performed by Hiss *et al* [17] and Addiego *et al* [18]. However, there is a significant difference in yield stress between experiments and simulations. Yield stress is defined here as the first stress point on the stress–strain curve where an increase in strain occurs without an increase in stress. The experimentally obtained yield stresses are between 20 and 30 MPa while in this simulation they are about 120 MPa. This is the same order of magnitude as found in other simulations, for instance [2–4]. As the yield stress increases with the strain rate, the simulations are expected to produce a higher yield stress than the experiments.

The effect of the strain rate is presented in figure 3 and is limited to deformation at the strain of 0.02% or 2% for calculating the Young’s modulus and Poisson’s ratio. The simulations show Hookean elasticity responses to the applied uniaxial load at low strains. Figure 3 indicates that the stiffness and yield stress increase with increasing strain rate. Hiss *et al* [17] and Addiego *et al* [18] also found that increasing strain rate increases the yield stress. Figure 4 presents the influence of temperature on the stress–strain behaviour. Decreasing temperature increases the stiffness and the yield stress.

The Young’s modulus and Poisson’s ratio values discussed in the following sections were obtained by averaging the values calculated from the stress–strain curves from the three simulations, in which the sample was elongated in the X, Y or Z direction in each simulation. The average values for different strain rates and temperatures are shown in table 2 together with the standard deviations. The standard deviations are reasonably low.

3.2. Effects of temperature and strain rate on the Young’s modulus

The Young’s modulus was calculated from the slope of the stress–strain curve below the linear limit, typically below a strain of 0.02% or 2%. For each combination of temperature and strain

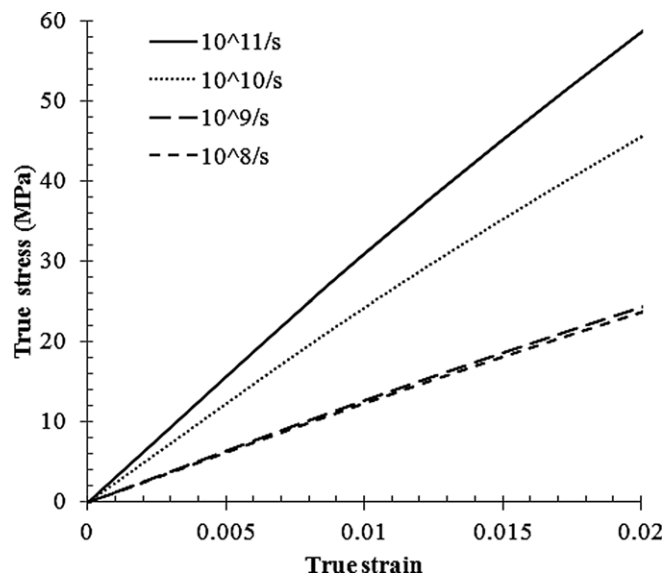


Figure 3. Effect of strain rate on the stress–strain curve at 200 K.

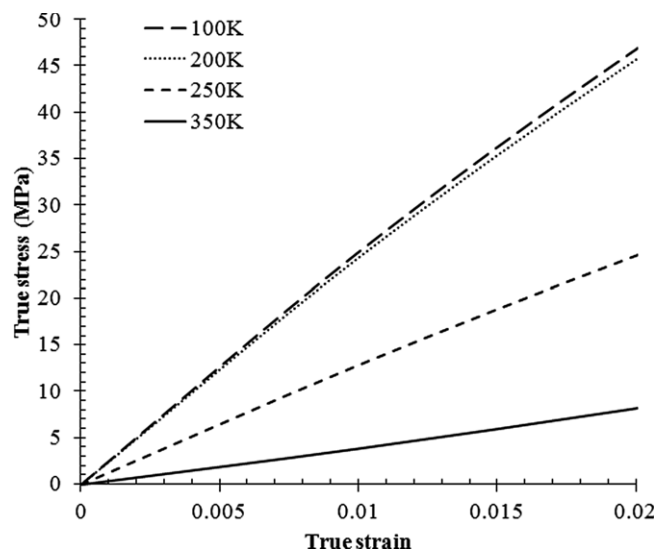


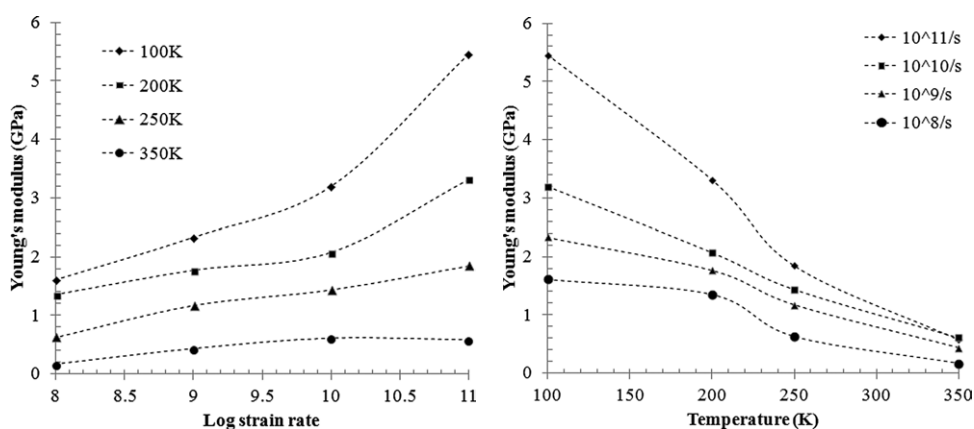
Figure 4. Effect of temperature on the stress–strain curve at a strain rate of 10^{10} s^{-1} .

rate, the Young's modulus values were obtained from three simulations and averaged. Table 2 shows the average value and standard deviation. Figure 5 presents the average value of the Young's modulus as a function of temperature and strain rate. Sigmoid curve fitting equations were applied to these average values to show the trend of the Young's modulus as a function of temperature.

Figure 5 indicates that the Young's modulus decreases with increasing temperature in all simulations. This dependence of stiffness on temperature has also been observed for other polymers, for instance, by Mahieux and Reifsnider [19] and Richeton *et al* [20]. The results

Table 2. Young's modulus and Poisson's ratio calculated from the simulations.

Strain rate (s^{-1})	Temperature (K)	Young's modulus (GPa)		Poisson's ratio	
		Average	Standard deviation	Average	Standard deviation
10^{11}	100	5.457	0.404	0.283	0.025
	200	3.313	0.961	0.277	0.022
	250	1.846	0.030	0.269	0.017
	350	0.579	0.195	0.265	0.005
10^{10}	100	3.198	0.200	0.326	0.051
	200	2.069	0.278	0.327	0.034
	250	1.438	0.319	0.339	0.042
	350	0.608	0.146	0.416	0.041
10^9	100	2.334	0.233	0.374	0.061
	200	1.765	0.106	0.397	0.042
	250	1.172	0.139	0.451	0.025
	350	0.429	0.192	0.482	0.107
10^8	100	1.609	0.199	0.385	0.025
	200	1.349	0.147	0.435	0.025
	250	0.625	0.005	0.504	0.083
	350	0.161	0.069	0.495	0.125

**Figure 5.** Effect of strain rate and temperature on Young's modulus.

also show that the simulation using a higher strain rate produces a higher Young's modulus compared with the simulation using a slower rate.

The results produced by the highest strain rate simulations ($10^{11} s^{-1}$) require careful attention. This strain rate is close to the vibrational frequency of PE, which is between 1.53×10^{12} and $8.76 \times 10^{13} s^{-1}$ according to [21]. Strain rates close to the vibrational frequencies may lead to errors in the molecular trajectories, with the result that the system may no longer have a normal structure. In each time step of the deformation process, the atomic positions are remapped following the change in the size of the simulation box at a constant strain rate. The changes of the atomic positions could be sufficiently large compared with the atomic oscillations, resulting in a discontinuous jump in the molecular bond distance without any physical meaning. Therefore, the $10^{11} s^{-1}$ simulation results will not be used in the subsequent analysis and discussion.

It is well known that the mechanical properties of polymers vary with both time and temperature. As indicated in figure 5, increasing the temperature affects the Young's modulus in a similar way as decreasing the strain rate. The time–temperature superposition based on this phenomenon is widely used to form a 'master curve' using a shift factor to superimpose mechanical properties measured at different temperatures. Experimental test results, such as the Young's moduli, are multiplied by a shift factor to produce a single master curve. The shift factor is determined experimentally with respect to a reference temperature.

The shift factor used to construct a master curve was experimentally determined for a large number of amorphous polymers by Williams, Landel and Ferry [22], who expressed the WLF equation:

$$\log_{10}a_T = \frac{-C_1(T - T_0)}{C_2 + (T - T_0)} \quad (2)$$

Equation (2) is an empirical equation found as an approximately identical shift factor–temperature relation for a wide variety of polymers, polymer solutions, organic glass-forming liquids and inorganic glasses. The theoretical basis to this equation is Doolittle's free volume [23] that is based on experimental data. The temperature dependence of viscosity arises largely from its dependence on free volume. The free volume is constant up to T_g and then increases linearly with increasing temperature. Equation (2) has been validated with higher strain rates than typical experimental test rates [24, 25]. But the strain rates were still much lower than typical MD simulation rates. Equation (2) is valid above the glass transition temperature (T_g) because below this temperature, $\log a_T$ increases less rapidly with decreasing temperature [22]. Using the WLF equation at much higher strain rates than used in laboratory experiments is an unproven approach, but, as discussed later, it can explain results from MD fairly well.

The values of the WLF constants C_1 and C_2 for these simulations were taken to be 15.0 and 50.5, respectively, from [26]. They were calculated using experimental results of an HDPE sample. The sample's T_g (= 155 K) was chosen as the reference temperature T_0 . Since our sample in the simulations was purely amorphous PE, the WLF constants for the HDPE sample with the lowest degree of crystallinity (40%) in [26] were chosen to be used for the calculation of the shift factor for our simulation results.

Bauwens *et al* [27] reported that the yield stress of glassy polymers below T_g can be described by the Eyring theory of non-Newtonian flow. The linear form of the Eyring equation is similar to the Arrhenius activation energy equation. The shift factor is given by

$$\log_{10}a_T = \frac{Q}{2.303R} \left[\frac{1}{T} - \frac{1}{T_0} \right] \quad (3)$$

where Q is the activation energy and R is the universal gas constant. The activation energy of linear PE is taken from [28] as 27 kJ mol^{-1} .

The Young's modulus values at different temperatures and strain rates obtained from the simulations were plotted against the shifted log strain rate from equation (2) for data at the temperature above T_g and from equation (3) for data at the temperature below T_g . The master curve at T_g (155 K) is presented in figure 6. This figure shows that the original log strain rate between 8 and 10 has been shifted to between about -4 and 5 . This indicates that the simulations predict Young's modulus behaviour in accordance with the time–temperature superposition principle.

Young's moduli calculated from the simulation results were compared with the values obtained by experimental measurements reported by Bucknall [29]. In his report, the Young's modulus was measured from HDPE samples using tensile tests over a range of strain rates and at different temperatures. The Young's modulus was found to increase with increasing strain

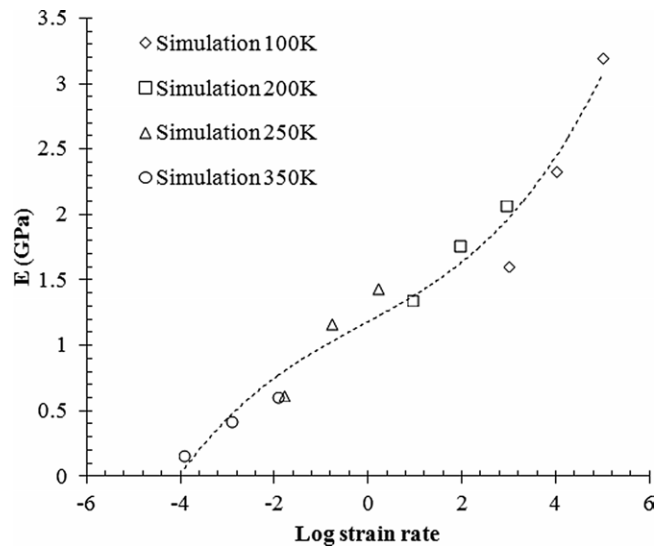


Figure 6. Master curve (dashed line) of Young's modulus.

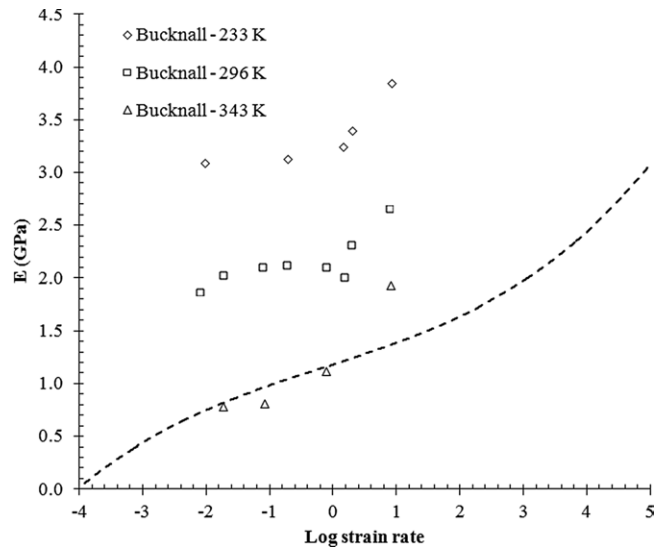


Figure 7. Comparison of Young's modulus as a function of strain rate from measurements by Bucknall [29] and the master curve (dashed line) of the simulation at T_g (155 K).

rate and decreasing temperature. Figure 7 compares measurements by Bucknall [29] and the master curve obtained from the simulations.

The WLF equation, equation (2), was again applied to the Young's modulus values of Bucknall [29] to form a master curve. The values of the constants C_1 and C_2 for the previous WLF equation could not be used because the samples studied by Bucknall [29] have degrees of crystallinity between 94% and 97%. Therefore, the C_1 and C_2 constants were assigned values of 8.86 and 101.6 based on [22], and the reference temperature (T_0) was set to 233 K. Over a range of temperatures between T_g and $T_g + 100$, these values are valid for a wide variety of polymers, polymer solutions, organic glass-forming liquids and inorganic glasses [22].

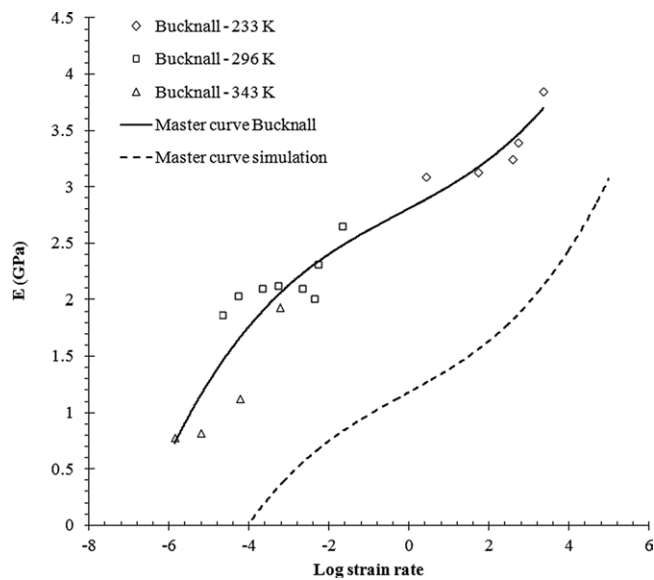


Figure 8. Comparison of the master curve of Bucknall [29] at 233 K (solid line) and the master curve of the simulation at 155 K (dashed line).

Figure 8 compares the master curve found by Bucknall with the simulation. The Young's moduli of these simulations are lower than those of the experiments, but the master curves have similar shapes.

HDPE has a high degree of crystallinity and a varying amount of amorphous structure. The elastic modulus increases approximately in proportion to the degree of crystallinity in a certain range [30–32]. In this simulation, the PE system is purely amorphous, while the HDPE in Bucknall's report has a degree of crystallinity between 94% and 97% as measured by Pranadi and Manuel [33]. According to Popli and Mandelkern [32], for degrees of crystallinity less than 25%, the moduli remain constant at approximately 20 MPa. Therefore, the degree of crystallinity leads to a difference in the Young's modulus between experimental measurements and the simulated results.

Semicrystalline PE has not only a crystalline region surrounded by a disordered (amorphous) region, but also an interfacial region that connects the two. Therefore, the elastic modulus will be affected both by the degree of crystallinity and by how the interfacial region connects the crystalline and amorphous regions.

Another possible reason for the discrepancy between the simulations and experimental measurements is the effect of molecular orientation. HDPE elongated in the solid state exhibits a strong dependence of the Young's modulus on molecular orientation, for instance as reported by Capaccio and Ward [34] and Capaccio *et al* [35]. Increasing the degree of orientation increases the Young's modulus. The experimental samples studied by Bucknall [29] were prepared by an injection moulding process and could have had higher degree of molecular orientation compared with the simulated samples.

3.3. Effects of temperature and strain rate on Poisson's ratio

In each simulation, a curve of transverse strain versus longitudinal strain was obtained and Poisson's ratio was calculated from the slope of the curve at a low strain. For each combination of temperature and strain rate, the Poisson's ratio values were obtained from three simulations

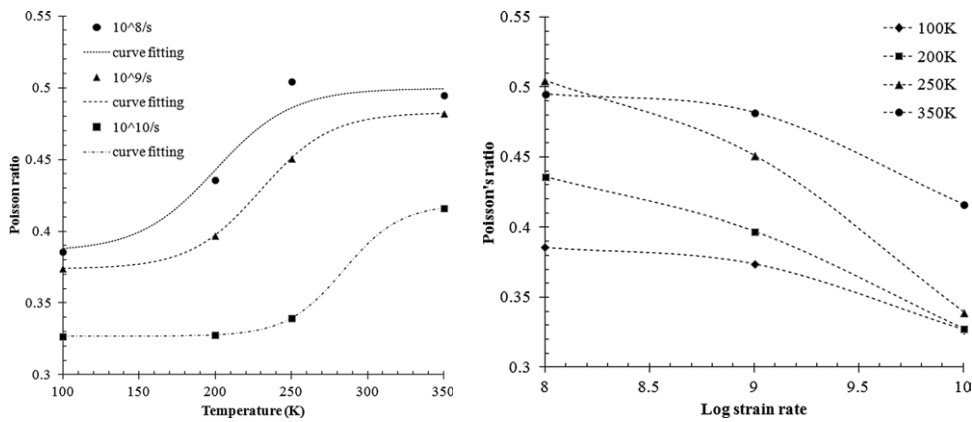


Figure 9. Effects of temperature and strain rate on Poisson's ratio.

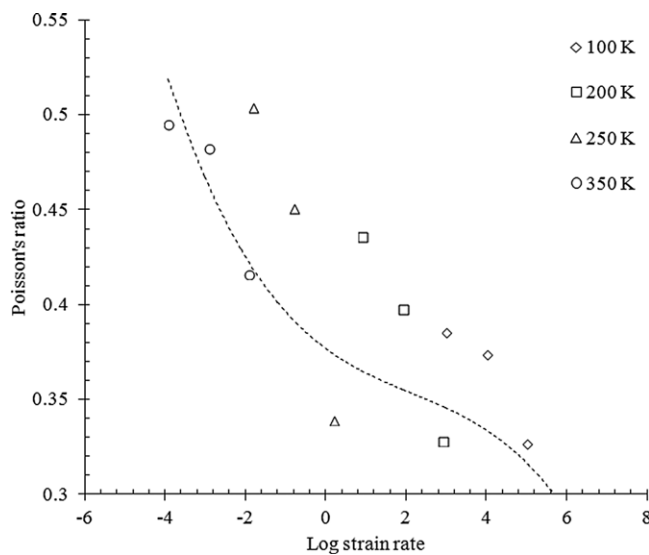


Figure 10. Master curve (dashed line) of Poisson's ratio.

and averaged. Table 2 shows the average value and standard deviation. Figure 9 presents the average value of Poisson's ratio as a function of temperature and strain rate. Again, the sigmoidal curve fitting equations were applied to these average values to show the trend of Poisson's ratio as a function of temperature.

Figure 9 indicates that in the simulations using strain rates of 10^8 , 10^9 and 10^{10} s^{-1} , Poisson's ratio increases with temperature following a sigmoidal trend. This trend is similar to the experimental results of other polymers reported by Seitz [36] for PC, PS, PMMA, PVT, ST/MMA, PVC and POMS; by Mott *et al* [37] for PS and PMMA; by Pandini and Pegoretti [38] for PBT and by Pandini and Pegoretti [39] for epoxy resins.

Poisson's ratio depends on the strain rate and temperature, as indicated in figure 9. In the same way as for the Young's modulus, equation (2) was used to calculate the log shift factor for Poisson's ratio at the temperature above T_g and equation (3) was used for the temperature below T_g . The Poisson's ratio master curve is presented in figure 10. These simulations are

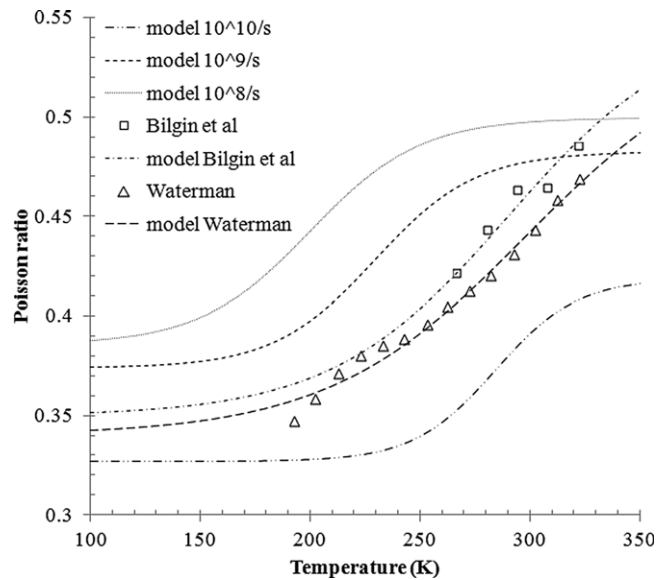


Figure 11. Comparison of Poisson's ratio from data measured by Bilgin *et al* [40], Waterman [41] and the simulation model.

able to produce the trend in Poisson's ratio following the time (or strain rate)–temperature superposition principle.

Poisson's ratios obtained from the simulation results were compared with experimental measurements. Bilgin *et al* [40] found that Poisson's ratio of the MDPE pipe at a strain rate close to $1000 \mu\epsilon \text{ min}^{-1}$ (approximately $1.6 \times 10^{-5} \text{ s}^{-1}$) increased from 0.42 at -6.7°C to 0.48 at 49°C . The equation of the curve fit to the simulation at a strain rate of 10^9 s^{-1} in figure 10 showed that Poisson's ratio was 0.464 at a temperature of -6.7°C (approximately 266 K), and 0.481 at 49°C (approximately 322 K).

Waterman [41] calculated the complex Poisson's ratio of six different samples of PE by measuring the velocity and attenuation of ultrasonic longitudinal and transverse pulses at a frequency of 5 MHz and a strain rate of approximately 10^2 s^{-1} . For comparison with the simulations, we used the real part of the complex Poisson's ratios of these measurements because the value of the real part is close to the time-dependent Poisson's ratio [42]. At -80°C , the experimental value of Poisson's ratio was 0.35, and at 50°C it was 0.47. In the simulations, Poisson's ratio was 0.39 at -80°C (approximately 193 K) and 0.48 at 50°C (approximately 323 K).

Figure 11 presents a comparison between the simulation and the experimental values of Poisson's ratio. Figure 11 shows that the trends of the effects of strain rate and temperature on Poisson's ratio in the simulations are similar to those in the experiments. The difference between Poisson's ratios measured experimentally and calculated in the simulations results from the same factors that influence the Young's modulus as discussed in the previous section.

4. Conclusion

Molecular dynamics simulations of the deformation of amorphous PE are performed at various engineering strain rates and temperatures. Comparisons of the effects of temperature and strain rate on the deformation responses between MD simulations and laboratory experiments are

presented and discussed. The stress–strain curves at a low strain obtained from the simulations have the same typical shapes as those obtained from laboratory experiments. The Young's modulus and Poisson's ratio values were calculated from the simulations showing the strain rate and temperature dependences and were in reasonable agreement with the experimental measurements.

The time (or strain rate)–temperature superposition principle was applied to the Young's modulus and Poisson's ratio to form master curves. These master curves can be used to bridge the difference between the high strain rates of the simulations and the much lower rates of the laboratory experiments. The differences in terms of the numbers of monomers and chains, the degree of crystallinity and the molecular orientation lead to discrepancies between the Young's modulus and Poisson's ratio values calculated from the simulations and those measured in laboratory experiments.

Acknowledgments

This research was financed by the Norwegian University of Science and Technology (NTNU). Computational resources at NTNU were partially provided by NOTUR, <http://www.notur.no>. This support is gratefully acknowledged.

References

- [1] ISO/TS 10839:2000, Polyethylene pipes and fittings for the supply of gaseous fuels—code of practice for design, handling and installation
- [2] Brown D and Clarke J H R 1991 Molecular dynamics simulation of an amorphous polymer under tension: I. Phenomenology *Macromolecules* **24** 2075–82
- [3] Yang L *et al* 1997 Extended ensemble molecular dynamics method for constant strain rate uniaxial deformation of polymer systems *J. Chem. Phys.* **107** 4396–407
- [4] Capaldi F M *et al* 2004 Molecular response of a glassy polymer to active deformation *Polymer* **45** 1391–9
- [5] Rottler J and Robbins M O 2003 Shear yielding of amorphous glassy solids: effect of temperature and strain rate *Phys. Rev. E* **68** 011507
- [6] Mahajan D K and Basu S 2010 On the simulation of uniaxial, compressive behaviour of amorphous, glassy polymers with molecular dynamics *Int. J. Appl. Mech.* **02** 515–41
- [7] Lyulin A V *et al* 2006 Atomistic simulation of bulk mechanics and local dynamics of amorphous polymers *Macromol. Symp.* **237** 108–18
- [8] Mayo S L *et al* 1990 DREIDING: a generic force field for molecular simulations *J. Phys. Chem.* **94** 8897–909
- [9] Lavine M S *et al* 2003 Molecular dynamics simulation of orientation and crystallization of polyethylene during uniaxial extension *Polymer* **44** 1771–9
- [10] Hossain D *et al* 2010 Molecular dynamics simulations of deformation mechanisms of amorphous polyethylene *Polymer* **51** 6071–83
- [11] Plimpton S J 1995 Fast parallel algorithms for short-range molecular dynamics *J. Comput. Phys.* **117** 1–19
- [12] Schneider T and Stoll E 1978 Molecular-dynamics study of a three-dimensional one-component model for distortive phase transitions *Phys. Rev. B* **17** 1302
- [13] Adelman S A and Dol J D 1976 Generalized Langevin equation approach for atom–solid–surface scattering—general formulation for classical scattering off harmonic solids *J. Chem. Phys.* **64** 2375–88
- [14] Gedde U W 1995 *Polymer Physics* (London: Chapman and Hall)
- [15] Nakajima A *et al* 1967 Unperturbed chain dimensions of polyethylene in theta solvents *J. Polym. Sci. C* **15** 285–94
- [16] Muraoka Y *et al* 1983 Direct determinations of the unperturbed dimensions of linear polyethylene molecules *Br. Polym. J.* **15** 107–9
- [17] Hiss R *et al* 1999 Network stretching, slip processes, and fragmentation of crystallites during uniaxial drawing of polyethylene and related copolymers. A comparative study *Macromolecules* **32** 4390–403
- [18] Addiego F *et al* 2006 Characterization of volume strain at large deformation under uniaxial tension in high-density polyethylene *Polymer* **47** 4387–99
- [19] Mahieux C A and Reifsnider K L 2001 Property modeling across transition temperatures in polymers: a robust stiffness–temperature model *Polymer* **42** 3281–91

- [20] Richeton J *et al* 2005 A unified model for stiffness modulus of amorphous polymers across transition temperatures and strain rates *Polymer* **46** 8194–201
- [21] Barrera G D *et al* 2006 The vibrational spectrum and ultimate modulus of polyethylene *Macromolecules* **39** 2683–90
- [22] Williams M L *et al* 1955 The temperature dependence of relaxation mechanisms in amorphous polymers and other glass-forming liquids *J. Am. Chem. Soc.* **77** 3701–7
- [23] Doolittle A K 1951 Studies in Newtonian flow: II. The dependence of the viscosity of liquids on free-space *J. Appl. Phys.* **22** 1471–5
- [24] Zhao J, Knauss W G and Ravichandran G 2007 Applicability of the time–temperature superposition principle in modeling dynamic response of a polyurea *Mech. Time-Depend. Mater.* **11** 289–308
- [25] Rauh A *et al* 2012 Application of the time–temperature superposition principle to the mechanical characterization of elastomeric adhesives for crash simulation purposes *Eur. Phys. J. Spec. Top.* **206** 15–24
- [26] Alberola N *et al* 1992 Mechanical γ and β relaxations in polyethylene: I. Glass transitions of polyethylene *Eur. Polym. J.* **28** 935–48
- [27] Bauwens J C *et al* 1969 Tensile yield-stress behavior of poly(vinyl chloride) and polycarbonate in the glass transition region *J. Polym. Sci. Part A-2* **7** 1745–54
- [28] Stadler F J *et al* 2008 Thermorheological behavior of various long-chain branched polyethylenes *Macromolecules* **41** 1328–33
- [29] Bucknall C B 1986 Application of fracture mechanics to the prediction of the ductile-brittle transition *Pure Appl. Chem.* **58** 999–1014
- [30] Peacock A J and Mandelkern L 1990 The mechanical properties of random copolymers of ethylene: force–elongation relations *J. Polym. Sci. B* **28** 1917–41
- [31] Kennedy M A *et al* 1994 Tensile properties of crystalline polymers: linear polyethylene *Macromolecules* **27** 5297–310
- [32] Popli R and Mandelkern L 1987 Influence of structural and morphological factors on the mechanical properties of the polyethylenes *J. Polym. Sci. B* **25** 441–83
- [33] Pranadi H and Manuel A J 1980 Application of wide line nuclear magnetic resonance to the determination of the crystallinities of isotropic polyethylenes *Polymer* **21** 303–8
- [34] Capaccio G and Ward I M 1975 Ultra-high-modulus linear polyethylene through controlled molecular weight and drawing *Polym. Eng. Sci.* **15** 219–24
- [35] Capaccio G *et al* 1975 Preparation of ultra-high modulus linear poly-ethylenes: effect of initial crystallization conditions *Polymer* **16** 469
- [36] Seitz J T 1993 The estimation of mechanical properties of polymers from molecular structure *J. Appl. Polym. Sci.* **49** 1331–51
- [37] Mott P H, Dorgan J R and Roland C M 2008 The bulk modulus and Poisson’s ratio of ‘incompressible’ materials *J. Sound Vib.* **312** 572–5
- [38] Pandini S and Pegoretti A 2011 Time and temperature effects on Poisson’s ratio of poly(butylene terephthalate) eXPRESS *Polym. Lett.* **5** 685–97
- [39] Pandini S and Pegoretti A 2008 Time, temperature, and strain effects on viscoelastic Poisson’s ratio of epoxy resins *Polym. Eng. Sci.* **48** 1434–41
- [40] Bilgin O *et al* 2007 Thermal and mechanical properties of polyethylene pipes *J. Mater. Civil Eng.* **12** 1043–52
- [41] Waterman H A 1963 Determination of the complex moduli of viscoelastic materials with ultrasonic pulse method (part II) *Kolloid-Z.u.Z.f. Polymere* **192** 9–16
- [42] Tschoegl N W *et al* 2002 Poisson’s ratio in linear viscoelasticity—a critical review *Mech. Time-Depend. Mater.* **6** 3–51